processes

MDPI

Article

The Use of a Vortex Generator for the Efficient Cooling of Lithium-Ion Batteries in Hybrid Electric Vehicles

Ankit Singh Bisht [1], Vijay Singh Bisht [1], Prabhakar Bhandari [2,*], Kamal Singh Rawat [3], Tabish Alam [4,*] and Paolo Blecich [5,*]

1 Department of Thermal Engineering, Faculty of Technology, Veer Madho Singh Bhandari Uttarakhand Technical University, Dehradun 248007, India
2 Mechanical Engineering Department, K. R. Mangalam University, Gurgaon 122103, India
3 Mechanical Engineering Department, MIET, Meerut 250005, India
4 CSIR—Central Building Research Institute, Roorkee 247667, India
5 Faculty of Engineering, University of Rijeka, 51000 Rijeka, Croatia
* Correspondence: prabhakar.bhandari40@gmail.com (P.B.); tabish.iitr@gmail.com (T.A.); paolo.blecich@riteh.hr (P.B.)

Abstract: High heat flux dissipation from the Lithium-ion battery pack of hybrid electric vehicles is one of the major concerns in the automotive sector, since it directly affects the performance and it may also lead to permanent failure. Among various thermal management systems, forced air cooling is most favorable due to its light weight, compactness, lower cost, and design flexibility. In the present work, a battery thermal management system with the two types of vortex generator in the coolant passage has been used to enhance the performance. A numerical model has been developed in commercial code to investigate the performance of the delta winglet and circular protrusion type vortex generator. Apart from that, both types of vortex generator have been compared in terms of various parameters such as pressure drop, weight, and maximum temperature. From the results of the simulation, it has been observed that both vortex generators performed better at the attack angle of 30° in comparison to the attack angles of 45° and 60°. Furthermore, it has also been found that the cooling system with protrusion as the vortex generator has performed better in terms of thermos-hydraulic performance compared to the cooling system with the delta winglet vortex generator. In addition to that, the protruded system is lighter in weight compared to both the plain and delta winglet systems, and is recommended.

Keywords: forced air cooling; hybrid electric vehicle; lithium-ion battery; vortex generator; delta winglet; protrusion

Citation: Bisht, A.S.; Bisht, V.S.; Bhandari, P.; Rawat, K.S.; Alam, T.; Blecich, P. The Use of a Vortex Generator for the Efficient Cooling of Lithium-Ion Batteries in Hybrid Electric Vehicles. *Processes* **2023**, *11*, 500. https://doi.org/10.3390/pr11020500

Academic Editor: Xiaopeng Li

Received: 10 January 2023
Revised: 29 January 2023
Accepted: 5 February 2023
Published: 7 February 2023

1. Introduction

The global demand for energy resources (particularly crude oil) keeps on increasing day by day and nearly two-thirds are taken up by the transportation sector. Additionally, the detrimental impact of conventional fuels on the environment triggers research into the development of various clean energy vehicles such as pure electric vehicles (EVs), hybrid electric vehicles (HEVs) and plug-in hybrid electric vehicle (PHEVs). Such vehicles are energy efficient compared to the conventional internal combustion engine. In addition to that, these vehicles do not produce any harmful pollutants or greenhouse gases. According to Anderson et al. [1], the use of electric vehicles would reduce greenhouse gas emissions by nearly 40% if renewable energy sources were used for electric power generation. Various power batteries have been suggested, such as nickel–iron, nickel–zinc, nickel–cadmium, lead–acid, sodium–sulphur, lithium-ion (Li-ion), etc. Among the various battery systems, Li-ion batteries have been considered the most promising battery because of having a higher energy density, higher efficiency, longer cycling life, low self-discharge rates, etc. [2]. In spite of these merits, Li-ion batteries have some demerits in terms of cost, calendar life,

safety concerns and temperature-based degradation [3]. Researchers are trying to mitigate these demerits by finding better electrode material.

The problem of proper thermal management for such battery systems has not been properly addressed until the present time. The poor thermal management of these battery systems can cause degraded performance, lesser life span, and issues pertaining to battery security. A lithium-ion battery can work in a temperature range from −20 °C to 60 °C [4], with optimum performance between −15 °C and 35 °C [5]. Motoch et al. [6] pointed out that with every degree increase in working temperature in the range of 30–40 °C, a decrease in the calendar life of the battery by almost two months was observed. As electric vehicles use a combination of Li-ion batteries to cope with the higher power requirement, so more appropriate thermal management systems need to be designed. The cooling system should also ensure that temperature uniformity is maintained inside the cell pack.

The battery cooling techniques opted for earlier by researchers were active cooling, passive cooling, forced convection (with air, liquid and solid–liquid phase change materials (PCM)), and thermoelectric element cooling [7]. Among these techniques, air and liquid cooling are widely implemented in electric vehicles due to lower cost, simplicity and the availability of the coolant. In recent years, various geometric designs and respective operating conditions have been optimized by researchers to augment the performance of the cooling system [8]. Furthermore, the air-cooling system has exclusive merits over the liquid cooling system, such as a small volume with simple structure, being lightweight, having higher design flexibility, higher reliability, lower maintenance, and direct and safe access to the coolant [9].

The inlet and outlet designs are among the important factors which affect the flow field. A bidirectional flow in the battery thermal management system (BTMS) was proposed by Yu et al. [10] to augment the air cooling efficiency. The system has two independent inlets and fans; one was for heat dissipation by conventional air ducts, while the other was to reduce heat accumulations in the battery pack center by jet cooling. They observe a decrease in the maximum temperature from 42.3 °C to 33.1 °C. E et al. [11] conducted a comparative study on inlet–outlet location, i.e., both on either same wall or on opposite walls, and reported that inlet and outlet location on opposite sides had better performance compared to the same side configuration. In similar work, Chen et al. [12] pointed out that, for better cooling efficiency, the inlet and outlet should be located at the middle of the plenum. Further, researchers have also studied the different orientations of battery packs in the cooling system. Xu and He [13] varied the airflow over for two different battery arrangements, i.e., horizontally arranged and vertically arranged. They pointed out that, in horizontal arrangements, the air flow path is shorter, which results in an augmented cooling effect. The air-based BTMS with different arrangements of battery packs (aligned, staggered and intersected) was studied experimentally by Fan et al. [14] for varying inlet velocity. It was found that aligned arrangement has shown the best thermal performance and temperature uniformity, followed by staggered and intersected orientation. Furthermore, it was also pointed out that with an increase in inlet velocity there is an exponential increase in parasitic power consumption, and reportedly the least power was consumed in aligned orientation. The influence of inlet and outlet angles and duct dimensions on cooling performance was analyzed by Xie et al. [15]. They reported that the best performance was achieved when inlet and outlet angles are 2.5° and duct widths are the same. The thermal characteristics of the battery pack are also significantly affected by the cell spacing. It was observed by Fan et al. [16] that lower cell spacing or higher flow rate results in a lesser maximum temperature, while a more uniform temperature was obtained with moderate cell spacing. Similar observations were also reported by Park et al. [17]. Mahamud and Park [18] utilized reciprocating air flow in their battery thermal management system to reduce maximum cell temperatures and improve temperature uniformity.

Sun and Dixon [19] numerically studied the z-shaped flow battery pack with uniform and tapered inlet and outlet ducts, as depicted in Figure 1a. They found that tapered inlet

and outlet ducts help in reducing the temperature rise trend. Further, inserting corrugated plates results in a reduction in the maximum temperature of the battery packs. Park [20] numerically studied various manifold designs for battery packs for U-shaped flow as depicted in Figure 1b. They concluded that tapered manifold and ventilation can help in heat transfer augmentation. It is worth mentioning that forced air cooling with different flow arrangements has demonstrated better performance; nevertheless, very limited works have been reported on the use of different techniques for heat transfer enhancement in the battery thermal management system. There are various types of vortex generators that have been employed in heat exchangers, such as ribs, protrusion, fins, delta winglets, etc. [21,22]. Moreover, work on forced air convection with a vortex generator has seldom been reported. Therefore, the main objective of the proposed work is to enhance the performance of forced air cooling with the aid of a delta winglet and protrusions vortex generator. Both vortex generators were compared in terms of various parameters, such as pressure drop, weight, and maximum temperature obtained.

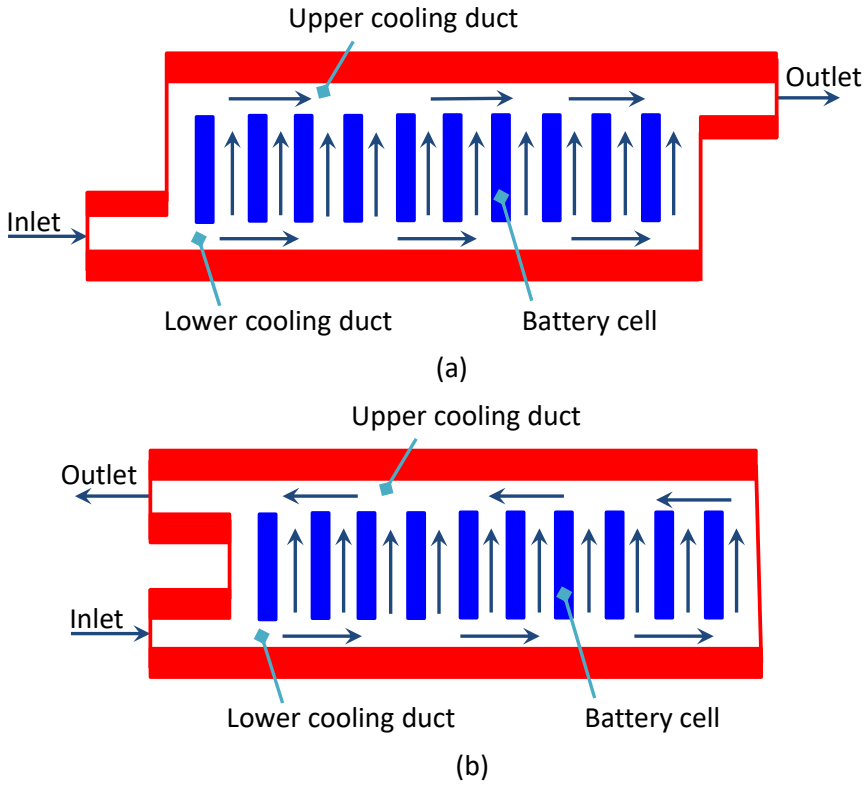

Figure 1. (**a**) Z-type flow arrangement [19]; (**b**) U-type flow arrangement [20].

2. Numerical Modelling

In the present work, the battery thermal management system considered is similar to Park [20]. The battery packs have 72 battery cells in two rows to operate 270 V and 1400 Wh. In each row, there are 36 battery cells and 37 fluid flow passages, as depicted in Figure 2a. The gap in between the battery cells is of 3 mm for the flow passage, so that a heat flux of 245 W/m^2 can be dissipated. The battery system has dimension of L × W × H = 787 mm × 225 mm × 191 mm, while the coolant passage size is 3 mm × 65 mm × 151 mm, as depicted in Figure 2b. The inlet and outlet manifold has dimension of 20 mm plenum and the first coolant passage is 100 mm away from the entrance and exit.

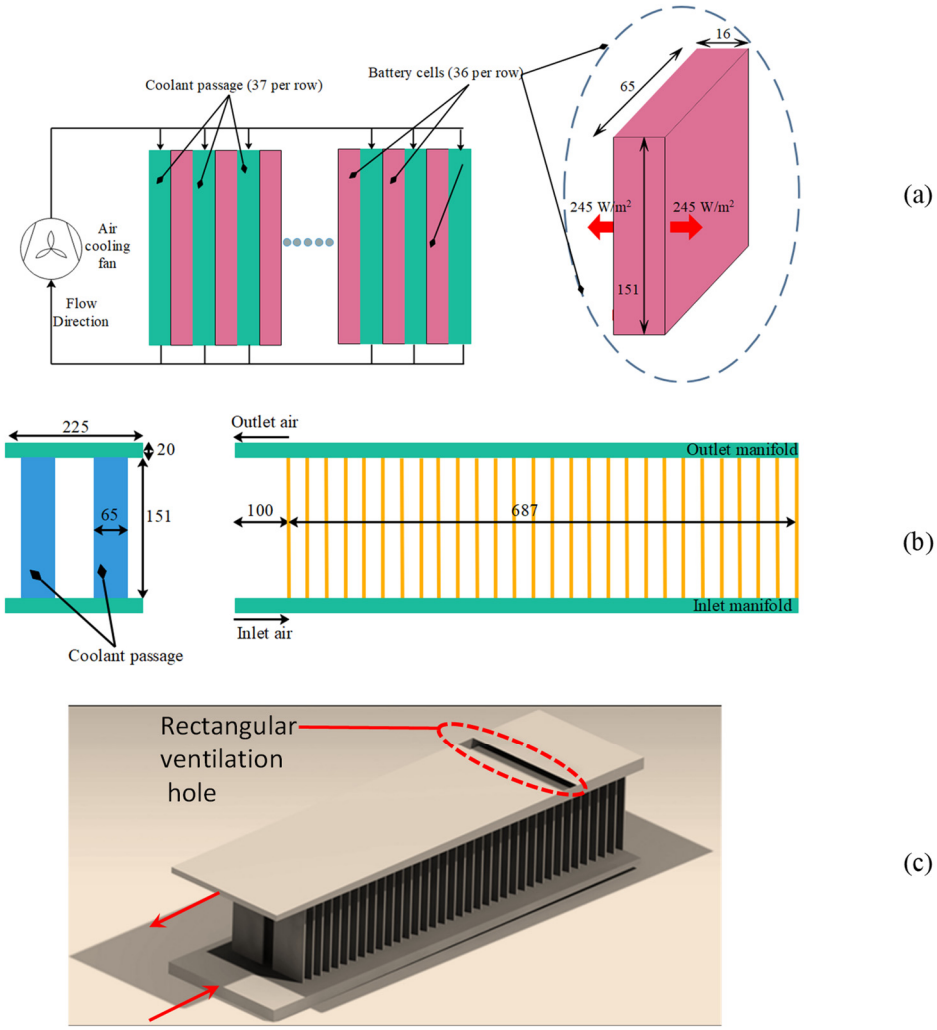

Figure 2. (**a**) Schematic diagram of battery thermal management system; (**b**) Sectional and side view of cooling system with complete specification; (**c**) Isometric diagram of type-V configuration by Park [20].

Park [20] considers five different configurations of the battery thermal management system configuration, based on manifold geometry. In his first geometry, the inlet and outlet plenum has a uniform cross section of 20 mm width throughout the length and is named as a type-I configuration; then, he modifies the manifold geometry in a tapered (converging or diverging) fashion and terms them type-II and -III configurations. For comparative purpose he also considered a uniform Z-shaped flow manifold (type-IV). Finally, there is the type-V configuration, i.e., modified type-III, where the type-III configuration has a rectangular ventilation hole (pressure relief) in the outlet manifold. Out of the five different configurations considered by Park [20], configuration type-V has been validated as it has shown the best performance among all five configurations and is also considered as reference geometry. The isometric diagram of the type-V configuration is shown in Figure 2c, and the same has also been used for validation purposes.

2.1. Solution Methodology

The numerical analysis in the present work has been carried out to see the influence of the vortex generator on the overall performance of BTMS. Commercially available CFD code ANSYS V16.0 has been opted for to perform the present work. Due to the complex nature of geometry, an unstructured mesh has been created over the computational domain. Using an ICEM module of ANSYS V 16.0, a polyhedral mesh with a fine prism layer has

been generated. The same geometry is considered as the reference configuration. After the discretization of the geometry, the problem is simulated using a fluent module. The boundary condition considered in present work is tabulated in Table 1. Various assumptions, such as no slip conditions at the channel passage wall, constant thermo-physical property for both coolant (air) and substrate (Aluminum) and incompressible air, have been considered to simplify the numerical analysis. The above-mentioned assumptions simplify the basic governing equations of fluid flow and heat transfer, i.e., continuity, Equation (1); momentum, Equation (2); and energy, Equation (3), as mentioned below.

$$\nabla \cdot (\rho_l \vec{V}) = 0 \tag{1}$$

$$\nabla \cdot (\rho_l \vec{V} \cdot \nabla \vec{V}) = -\nabla p + \nabla \cdot \mu_l [(\nabla \vec{V} + \nabla \vec{V}^t) - 2/3 \nabla \cdot \vec{V}] + \rho_l \vec{g} \tag{2}$$

$$\nabla \cdot (\rho_l c_{p,l} (\vec{V} T_l) = \nabla \cdot (k_l \nabla T_l) \tag{3}$$

where ρ_l, μ_l, k_l and $C_{p,l}$ represent density, viscosity, thermal conductivity and the specific heat of the coolant, respectively; $\vec{V}$, p and T are the symbols for velocity matrix, pressure and temperature. The superscript t is for the transpose of the particular matrix and subscript l represents the working fluid.

Table 1. Boundary conditions opted for in the present simulation.

S. No.	Boundary Zone	Zone Type	Boundary Conditions
1.	Inlet	Velocity inlet	Mass flow rate = 0.045 kg/s, temperature = 40 °C
2.	Outlet	Pressure outlet	Atmospheric pressure
3.	Bottom duct wall	Wall	No slip and adiabatic boundary conditions
4.	Top heated wall	Wall	No slip wall and uniform constant heat flux, q = 245 W/m^2

Among various models, the K-ε model is used for turbulent flow modelling in the numerical simulation. Taking the inlet velocity of 3.65 m/s, the different parameters have been evaluated. Thermal resistance has been calculated by the expression given in Equation (4), which is the ratio of temperature difference ($T_{max} - T_{min}$) to the heat flux (q).

$$R_{thermal} = \frac{T_{max} - T_{min}}{q} \tag{4}$$

The thermal resistance can be divided into two parts, i.e., convection thermal resistance and advection thermal resistance. Convection thermal resistance is due to the temperature difference between the coolant (air) and convective area (coolant passage wall), while the advection thermal resistance is due to a rise in the temperature of the air due to heat absorption.

$$R_{thermal} = R_{convection} + R_{advection} = \frac{1}{2Ah} + \frac{1}{Q\rho_l C_{p,l}} \tag{5}$$

where A is the area and h is the heat transfer coefficients, while in advection term Q is the flow rate of the working fluid (air), respectively. The Nusselt number has been calculated by Equation (6).

$$Nu = \frac{hD_h}{k_l} \tag{6}$$

where D_h is the hydraulic diameter, respectively. Pressure drop (Δp) is the difference in inlet and outlet pressure values.

The grid size in the Park [20] configuration has been varied from 1.9 million to 2.4 million in four steps for the grid independence test. It was observed that the average Nusselt number has shown negligible variation (less than 1%) after 2.4 million, so this grid size is considered for further calculations.

2.2. Validation

The present model is validated with the numerical work of Park [20]. For that, similar geometry has been created and simulated under similar operating conditions. The comparative contour for various parameters, (a) temperature distribution, (b) velocity distribution and (c) pressure contour, from both studies, is depicted in Figure 3. The deviation in maximum temperature and pressure drop from both studies is 1.42% and 4.01%, respectively. In addition to the contour plot, air flow rate distribution and thermal resistance in the individual coolant passage have also been compared and are found to be in good agreement with each other.

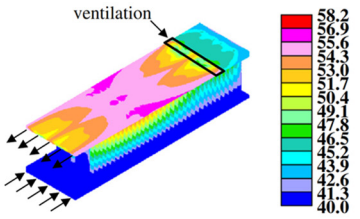

(a)-1 Temperature distribution from Park (2013)

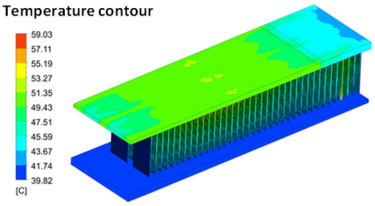

(a)-2 Temperature distribution from present simulation

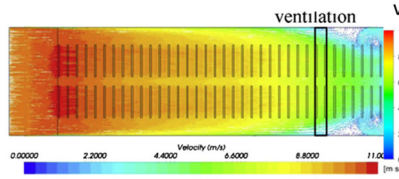

(b)-1 Velocity distribution in inlet manifold from Park (2013)

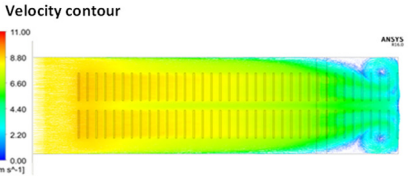

(b)-2 Velocity distribution inlet manifold from present simulation

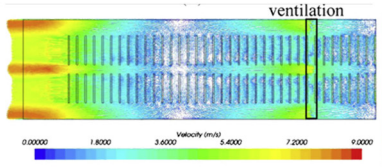

(c)-1 Velocity distribution in outlet manifold from Park (2013)

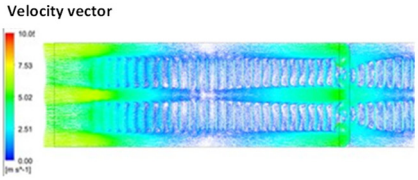

(c)-2 Velocity distribution in outlet manifold from present work

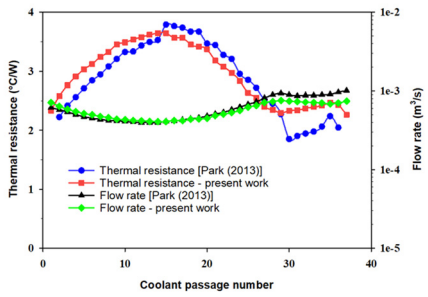

(d) Thermal resistance and air flow rate distribution in coolant passage

Figure 3. Validation of Park [20]'s configuration with present work.

3. Vortex Generator

To further augment the performance of the Park [20] configuration, modification in the form of a vortex generator has been proposed. The vortex generators have been used to enhance heat transfer characteristics by flow disruptions. Various applications such as heat exchangers, heat sinks, etc., use vortex generators, viz., delta winglet, twisted tape insert, ribs, fins, dimple, protrusion, etc. Among various vortex generators, it was observed that delta winglet and protrusion vortex generators are more suitable for coolant passage in BTMS. Therefore, these vortex generators are considered in the present study in the best observed configuration of Park [20], i.e., BTMS having a tapered inlet and outlet manifold with a ventilation hole in the outlet manifold. Firstly, the use of the vortex generator has been simulated for single coolant passage for a different attack angle, so that optimum geometry can be used in full scale BTMS.

Delta Winglet and Protrusion in Individual Coolant Passage

In the present model, delta winglets in two pairs are modelled on one side of the coolant passage, as depicted in Figure 4a. Three different attack angles are considered, varying from 30° to 60° as depicted in Figure 4b–d. It was performed to optimize the geometry of BTMS, so that the maximum heat transfer is obtained with the minimal pressure drop across the passage. The detailed parameters of the vortex generator are tabulated in Table 2. Figure 4e shows the meshed image of the coolant passage with the explored view in the vicinity of the delta winglet vortex generator. Due to the complex nature of the geometry, the domain is discretized using the ANSYS ICEM module. In the vicinity of the delta winglet, a fine-tuned prism layer has been created so that the mesh quality is not reduced and the boundary phenomenon near the wall is captured. Five different sets of meshes having numbers of elements of 182,881, 267,050, 320,155, 470,346 and 526,550 have been simulated for a grid independence test. On comparing the heat transfer coefficient, a slight variation, i.e., 0.25%, is observed in the last two grid sizes. Furthermore, the grid size with 470,346 numbers of elements has shown a y^+ value of 1. Therefore, the mesh with a number of elements of 470,346 is chosen in the study. Furthermore, complete details of the grid independence test for the delta winglet configuration have been tabulated in Table 4.

Table 2. Design parameters of the delta winglet vortex generator.

S. No.	Design Parameters	Value
1.	Flow angle of attack (α)	30°, 45° and 60°
2.	Winglet height (a)	2.5 mm
3.	Hydraulic diameter of the coolant passage (D_h)	5.74 mm
4.	Winglet aspect ratio ($\sigma = b/a$)	4
5.	Gap between winglet tip (δ)	3.75 mm
6.	e/D ratio	0.435

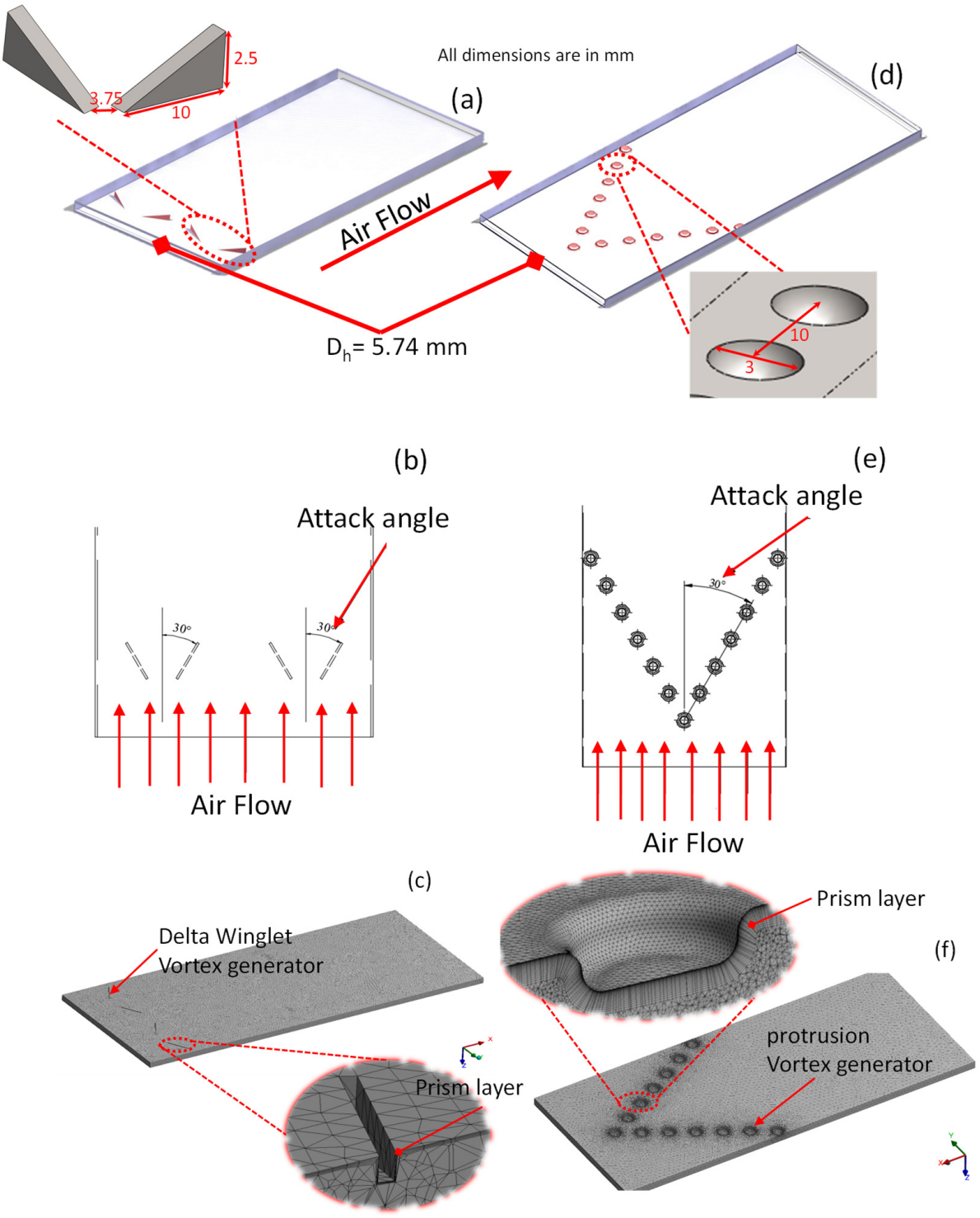

Figure 4. (**a**) Isometric view of cooling passage with delta winglet; (**b**) Top view of coolant passage with attack angle; (**c**) Meshed image of cooling passage with explored view around the delta winglet; (**d**) Isometric view of cooling passage with protrusion; (**e**) Top view of coolant passage having attack angle; (**f**) Meshed image of cooling passage with explored view around the protrusion.

Another vortex generator, circular protrusion, as shown in Figure 4d, has been used in the present study to compare the performance. Compared to the delta winglet, the protrusion in the coolant passage is easier to fabricate. This is because it can be made by a stamping process, and also there is no requirement for extra material, which can be helpful in weight reduction. Similar to the delta winglet, circular protrusion has been examined for different sets of attacking angle varying from 30° to 60°, as depicted in Figure 4e. In both configurations, the angles of attack were varied in a particular range only as it was reported in the literature that optimum performance was found in this range [23,24]. The detailed parameters of the circular protruded individual cooling passage are tabulated in Table 3.

Table 3. Design parameters of the protrusion vortex generator.

S. No.	Design Parameter	Value
1.	Flow angle of attack (α)	30°, 45° and 60°
2.	Height of the protrusion (e)	1 mm
3.	Hydraulic diameter of the coolant passage (D_h)	5.74 mm
4.	Protrusion diameter (d)	3 mm
5.	Gap between two protrusions (δ)	10 mm
6.	e/D ratio	0.174

The coolant passage has been meshed with tetrahedral elements, having a prism layer near the circular protrusion as depicted in Figure 4f. Five different sets of meshes having numbers of elements of 1,768,332, 1,931,802, 2,240,152, 2,532,934 and 2,788,706 have been opted for in the grid independence test. It was observed that, after the 2,532,934 number of elements, the increase in the heat transfer coefficient did not change significantly, so it was considered in further study. Furthermore, complete details related to the grid independence test are tabulated in Table 4.

Table 4. Grid independence test for delta winglet vortex generator and protrusion vortex generator.

	Delta Winglet Vortex Generator		Protrusion Vortex Generator	
S. No.	Number of Elements	% Variation in Heat Transfer Coefficients	Number of Elements	% Variation in Heat Transfer Coefficients
1.	182,881	-	1,768,332	-
2.	267,050	12%	1,931,802	11.3%
3.	320,155	5.6%	2,240,152	7.56%
4.	470,346	3.52%	2,532,934	2.3%
5.	526,550	0.25%	2,788,706	0.84%

It was observed that as the attacking angle increases from 30° to 60°, the wake region on the trailing side of the winglets kept on increasing and flow obstruction to the air flow also increased, which resulted in increased pressure drop. Figure 5a shows the effect of the attacking angle on thermal resistance, Nusselt number and pressure drop. Among three different attacking angles, the 30° showed superior performance and is recommended for full scale configuration.

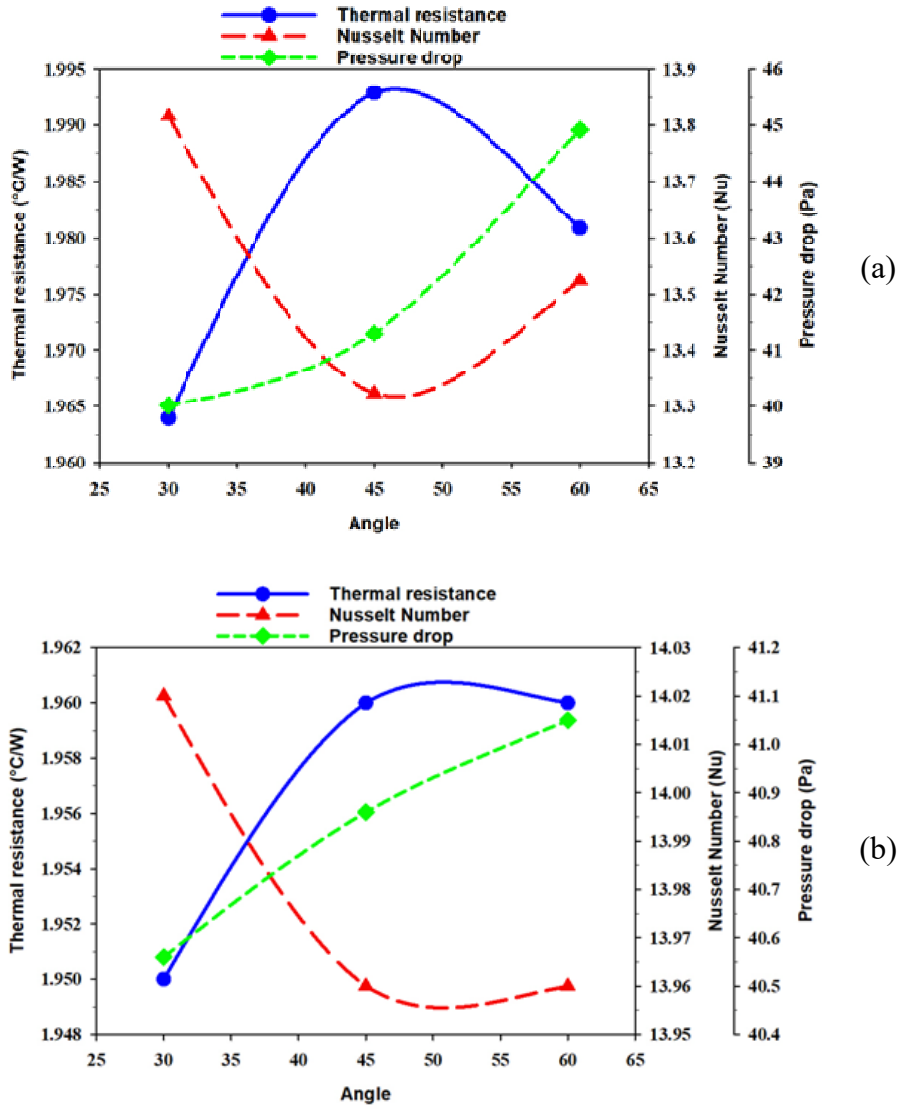

Figure 5. Effect of attack angle on thermo-hydraulic behavior for (**a**) delta winglet shaped vortex generator and (**b**) protrusion shaped vortex generator.

The influence of attack angle on the thermo-hydraulic performance has been plotted in Figure 5b. Similar to delta winglet, the 30° also showed better performance here and is recommended for a full-scale model of BTMS. The weight estimation has also been carried out on both coolant passages. The coolant passage with the delta winglet has shown a weight of 0.055 kg, while with protrusion the weight is 0.028 (approx. half compared to the delta winglet). In terms of the Nusselt number, the protruded coolant passage has shown better thermal characteristics compared to the coolant passage with the delta winglet. Furthermore, the pressure drop does not vary much in both vortex generators.

4. Full Scale Battery Thermal Management System with Vortex Generator

The individual coolant passage has shown optimized performance at the attacking angle of 30° and the same has been incorporated for a full-scale model. Battery thermal management systems with the delta winglet and protrusion as the vortex generator have been simulated under similar operating condition as were opted for in the reference configuration, i.e., Park [20].

Both systems have been simulated to visualize the overall performance. The temperature contour and air flow distribution for BTMS with the delta winglet are shown in Figure 6a,b, respectively. The BTMS with delta winglet has shown a maximum temperature of 53.63 °C, which is 5.4 °C (9.15%) less than plain BTMS. However, this increased performance happens at the expense of an increased pressure drop. The BTMS with circular protrusion has performed better than the BTMS with the delta winglet, as it has a 1.13 °C lesser maximum temperature. Temperature contour and flow distribution for the circular protrusion BTMS are depicted in Figure 6c,d, respectively.

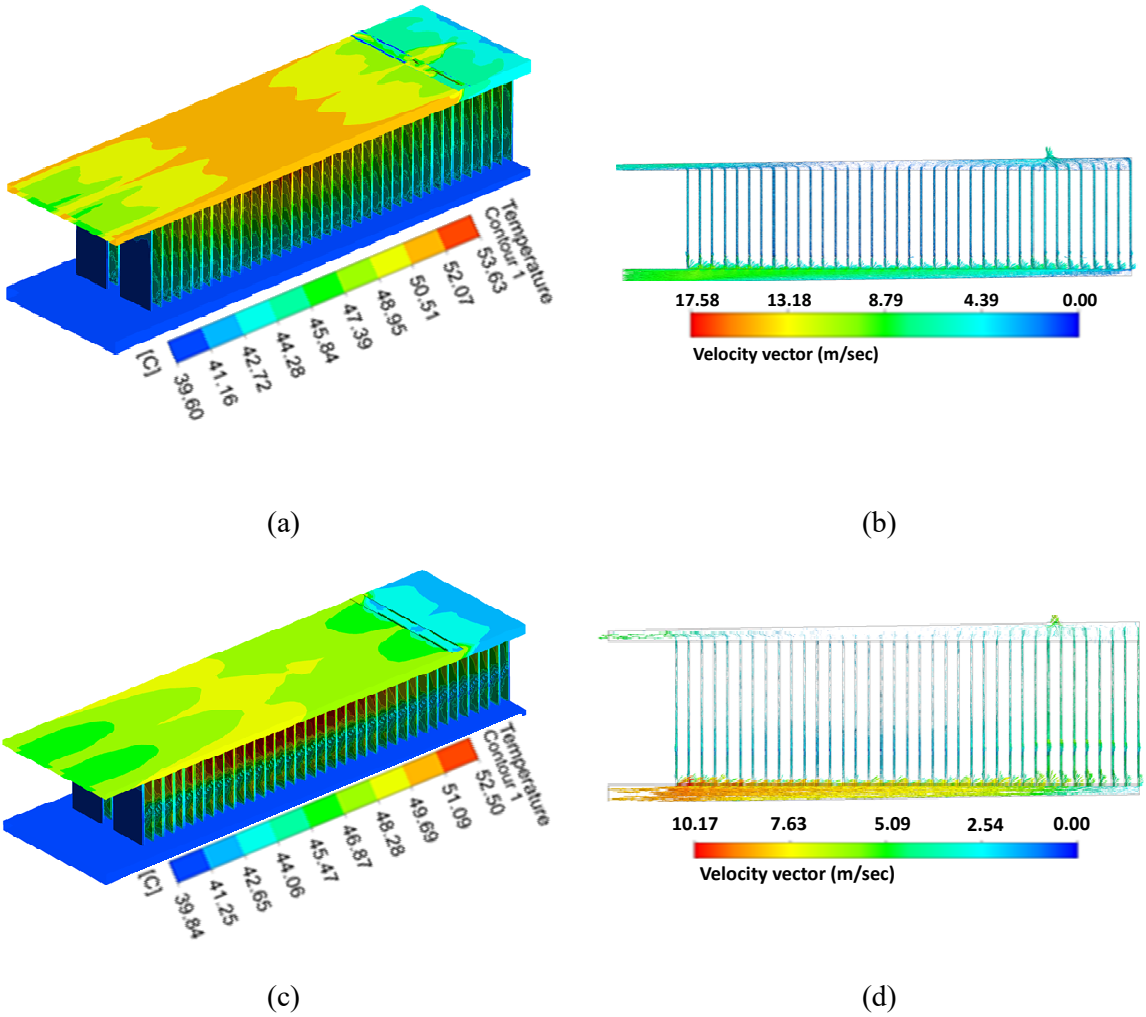

Figure 6. (**a**) Temperature contour in delta winglet BTMS; (**b**) Air flow distribution in delta winglet BTMS; (**c**) Temperature contour in protruded BTMS; (**d**) Air flow distribution in protruded BTMS.

In vehicles, the weight of the system plays an important role in its suitability. Considering the built material for different configurations as aluminum, the overall weight has been calculated. It was observed that the BTMS with the delta winglet is heaviest, followed by the reference configuration and protruded BTMS. The reference configuration has a mass of 4.087 kg, while the delta winglet BTMS has an overall mass of 6.084 kg and the protrusion BTMS has an overall mass of 4.027 kg. Moreover, the use of the delta winglet in the coolant passage makes the system bulky and expensive due to surplus material needs to be machined onto the design. On the contrary, the protrusion geometry is lightest and can be easily implemented.

The performances of all three systems are compared on the basis of pressure drop and maximum temperature, and this is tabulated in Table 5. The use of the delta winglet has shown a 16.2% increase in pressure drop, while protrusion geometry has shown an approx. 6.85% increase in pressure drop compared to the reference configuration, while in terms of maximum temperature the delta winglet had 9.15% and protrusion has shown 11.06% lesser value when compared to the reference geometry. Among all configurations, the cooling system with the protrusion vortex generator has shown the optimum performance compared to the other two configurations.

Table 5. Summary of the simulation results for the designed configuration.

	Reference Geometry [20]	BTMS with Delta Winglet	BTMS with Protrusion
ΔP (Pa)	67.4	80.4	72.02
Maximum Temperature (°C)	59.03	53.63	52.5

5. Conclusions

Battery thermal management systems play a crucial role in the effective operation of Lithium-ion battery packs in hybrid electric vehicles. If a higher temperature prevails in such systems, it can cause poor performance, permanent failure, and safety issues. In the present work, the cooling performance of various systems has been analyzed numerically. The present model has been validated by the numerical work of Park [20]. Commercial code ANYS Fluent V16.0 has been used to simulate the model, while the meshing was carried out in the ICEM module. Then, modification in the form of a vortex generator has been introduced in such systems. Two vortex generators, i.e., delta winglet and circular protrusion, were studied. The present study is divided into two parts. Firstly, the individual cooling passage was studied for different attack angles. It was found that an attack angle of 30° has shown better performance for configuration. Then, considering an attack angle of 30°, the full scale system was simulated. It was found that a battery thermal management system with circular protrusion performed better than the system with the delta winglet. In addition to that, the weight of the protruded BTMS is lesser, which is also helpful from a vehicle perspective.

Author Contributions: Conceptualization, A.S.B. and V.S.B.; methodology, A.S.B., V.S.B., P.B. (Prabhakar Bhandari) and K.S.R.; software, A.S.B., V.S.B., K.S.R. and P.B. (Prabhakar Bhandari); validation, A.S.B., V.S.B., P.B. (Prabhakar Bhandari) and K.S.R.; formal analysis, A.S.B., V.S.B., P.B. (Prabhakar Bhandari) and K.S.R.; investigation, A.S.B., V.S.B., P.B. (Prabhakar Bhandari) and K.S.R.; data curation, A.S.B., V.S.B., P.B. (Prabhakar Bhandari) and K.S.R.; writing—original draft preparation, A.S.B., V.S.B., P.B. (Prabhakar Bhandari) and K.S.R.; writing—review and editing, P.B. (Paolo Blecich), T.A. and K.S.R.; visualization, A.S.B., V.S.B. and P.B. (Paolo Blecich); supervision, P.B. (Paolo Blecich) and T.A.; project administration, P.B. (Paolo Blecich) and T.A. All authors have read and agreed to the published version of the manuscript.

Funding: This research received no external funding.

Data Availability Statement: Not applicable.

Conflicts of Interest: The authors declare no conflict of interest.

References

1. Andersen, P.H.; Mathews, J.A.; Rask, M. Integrating private transport into renewable energy policy: The strategy of creating intelligent recharging grids for electric vehicles. *Energy Policy* **2009**, *37*, 2481–2486. [CrossRef]
2. Liu, H.; Wei, Z.; He, W.; Zhao, J. Thermal issues about Li-ion batteries and recent progress in battery thermal management systems: A review. *Energy Convers. Manag.* **2017**, *150*, 304–330. [CrossRef]
3. Conte, F.V. Battery and battery management for hybrid electric vehicles: A review. *EI Elektrotech. Inf.* **2006**, *123*, 424–431. [CrossRef]
4. Väyrynen, A.; Salminen, J. Lithium ion battery production. *J. Chem. Thermodyn.* **2012**, *46*, 80–85. [CrossRef]

5. Pesaran, A.; Santhanagopalan, S.; Kim, G.H. *Addressing the Impact of Temperature Extremes on Large Format Li-ion Batteries for Vehicle Applications*; National Renewable Energy Lab. (NREL): Golden, CO, USA, 2013.
6. Motloch, C.G.; Christophersen, J.P.; Belt, J.R.; Wright, R.B.; Hunt, G.L.; Sutula, R.A.; Duong, T.; Tartamella, T.J.; Haskins, H.J.; Miller, T.J. High-power battery testing procedures and analytical methodologies for HEV's. *SAE Trans.* **2002**, *111*, 797–802.
7. Shahjalal, M.; Shams, T.; Islam, M.E.; Alam, W.; Modak, M.; Hossain, S.B.; Ramadesigan, V.; Ahmed, M.R.; Ahmed, H.; Iqbal, A. A review of thermal management for Li-ion batteries: Prospects, challenges, and issues. *J. Energy Storage* **2021**, *39*, 102518. [CrossRef]
8. Yang, N.; Zhang, X.; Li, G.; Hua, D. Assessment of the forced air-cooling performance for cylindrical lithium-ion battery packs: A comparative analysis between aligned and staggered cell arrangements. *Appl. Therm. Eng.* **2015**, *80*, 55–65. [CrossRef]
9. Westbrook, M.; Westbrook, M. *The Electric Car: Development and Future of Battery, Hybrid and Fuel-Cell Cars*; Institution of Electrical Engineers: London, UK, 2001.
10. Yu, K.; Yang, X.; Cheng, Y.; Li, C. Thermal analysis and two-directional air flow thermal management for lithium-ion battery pack. *J. Power Sources* **2014**, *270*, 193–200. [CrossRef]
11. Jiaqiang, E.; Yue, M.; Chen, J.; Zhu, H.; Deng, Y.; Zhu, Y.; Zhang, F.; Wen, M.; Zhang, B.; Kang, S. Effects of the different air cooling strategies on cooling performance of a lithium-ion battery module with baffle. *Appl. Therm. Eng.* **2018**, *144*, 231–2241.
12. Chen, K.; Wu, W.; Yuan, F.; Chen, L.; Wang, S. Cooling efficiency improvement of air-cooled battery thermal management system through designing the flow pattern. *Energy* **2019**, *167*, 781–790. [CrossRef]
13. Xu, X.M.; He, R. Research on the heat dissipation performance of battery pack based on forced air cooling. *J. Power Sources* **2013**, *240*, 33–41. [CrossRef]
14. Fan, Y.; Bao, Y.; Ling, C.; Chu, Y.; Tan, X.; Yang, S. Experimental study on the thermal management performance of air cooling for high energy density cylindrical lithium-ion batteries. *Appl. Therm. Eng.* **2019**, *155*, 96–109. [CrossRef]
15. Xie, J.; Ge, Z.; Zang, M.; Wang, S. Structural optimization of lithium-ion battery pack with forced air cooling system. *Appl. Eng.* **2017**, *126*, 583–593. [CrossRef]
16. Fan, L.; Khodadadi, J.M.; Pesaran, A.A. A parametric study on thermal management of an air-cooled lithium-ion battery module for plug-in hybrid electric vehicles. *J. Power Sources* **2013**, *238*, 301–312. [CrossRef]
17. Park, S.; Jung, D. Battery cell arrangement and heat transfer fluid effects on the parasitic power consumption and the cell temperature distribution in a hybrid electric vehicle. *J. Power Sources* **2013**, *227*, 191–198. [CrossRef]
18. Mahamud, R.; Park, C. Reciprocating air flow for Li-ion battery thermal management to improve temperature uniformity. *J. Power Sources* **2011**, *196*, 5685–5696. [CrossRef]
19. Sun, H.; Dixon, R. Development of cooling strategy for an air cooled lithium-ion battery pack. *J. Power Sources* **2014**, *272*, 404–414. [CrossRef]
20. Park, H. A design of air flow configuration for cooling lithium ion battery in hybrid electric vehicles. *J. Power Sources* **2013**, *239*, 30–36. [CrossRef]
21. Singh, B.P.; Bisht, V.S.; Bhandari, P.; Rawat, K. Thermo-Fluidic Modelling of a Heat Exchanger Tube with Conical Shaped Insert having Protrusion and Dimple Roughness. *Aptisi Trans. Technopreneurship* **2021**, *3*, 13–29. [CrossRef]
22. Singh, B.P.; Bisht, V.S.; Bhandari, P. Numerical Study of Heat Exchanger Having Protrusion and Dimple Roughened Conical Ring Inserts. In *Advances in Fluid and Thermal Engineering*; Lecture Notes in Mechanical Engineering; Sikarwar, B.S., Sundén, B., Wang, Q., Eds.; Springer: Singapore, 2021; pp. 151–161.
23. Chamoli, S.; Lu, R.; Xu, D.; Yu, P. Thermal performance improvement of a solar air heater fitted with winglet vortex generators. *Solar Energy* **2018**, *159*, 966–983. [CrossRef]
24. Yadav, S.; Kaushal, M. Nusselt number and friction factor correlations for solar air heater duct having protrusions as roughness elements on absorber plate. *Exp. Therm. Fluid Sci.* **2013**, *44*, 34–41. [CrossRef]